Acta Pharmaceutica Sinica B 2021;11(9):2914–2923

Chinese Pharmaceutical Association
Institute of Materia Medica, Chinese Academy of Medical Sciences

Acta Pharmaceutica Sinica B

www.elsevier.com/locate/apsb
www.sciencedirect.com

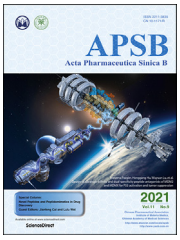

ORIGINAL ARTICLE

Simultaneous improvement to solubility and bioavailability of active natural compound isosteviol using cyclodextrin metal-organic frameworks

Xiaojin Chen[a,b,†], Tao Guo[b,†], Kaikai Zhang[b,c], Jiacai Chen[b,d], Caifen Wang[b], Xiaohong Ren[b], Qin Wang[a,b], Yingchao Yang[b], Chongjing Liu[b], Wen Tan[e], Shuangying Gui[a,*], Li Wu[b,*], Jiwen Zhang[a,b,c,d,*]

[a]*Anhui University of Traditional Chinese Medicine, Anhui 230000, China*
[b]*Center for Drug Delivery Systems, Shanghai Institute of Materia Medica, Chinese Academy of Sciences, Shanghai 201210, China*
[c]*Key Laboratory of Modern Preparation of TCM, Ministry of Education, Jiangxi University of Chinese Medicine, Nanchang 330004, China*
[d]*Nanjing University of Traditional Chinese Medicine, Nanjing 210000, China*
[e]*Institute of Biomedical and Pharmaceutical Sciences, Guangdong University of Technology, Guangzhou 510006, China*

Received 7 February 2021; received in revised form 1 April 2021; accepted 6 April 2021

KEY WORDS

Isosteviol;
Cyclodextrin metal-organic framework;
Drug loading;
Nanoclusters;
Solubility;
Bioavailability;

Abstract Cyclodextrin metal-organic framework (CD-MOF) as a highly porous supramolecular carrier could be one of the solutions to the insolubility of isosteviol (STV). The solubility of STV was lower than 20.00 ng/mL at pH 1.0 and pH 4.5, whilst its solubility increased to 20,074.30 ng/mL at pH 6.8 and 129.58 ng/mL in water with a significant pH-dependence. The *in vitro* release profiles of STV from STV@CD-MOF (0.5:1) were pH-independent in distinct pH media and closed to be thoroughly released but no such release profiles were observed for STV@CD-MOF (1:1) owing to nanoclusters formation. The bioavailability of STV@CD-MOF (1:1) in rats was 8.67-fold higher than that of STV, and was 1.32- and 1.27-fold higher than that of STV@CD and STV@CD-MOF (0.5:1). Our results indicated that

*Corresponding authors. Tel./fax: +86 21 50805901 (Jiwen Zhang); +86 21 20231980 (Li Wu); +86 551 68129123 (Shuangying Gui).
E-mail addresses: guishy0520@ahtcm.edu.cn (Shuangying Gui), wuli@simm.ac.cn (Li Wu), jwzhang@simm.ac.cn (Jiwen Zhang).
†These authors made equal contributions to this work.
Peer review under responsibility of Chinese Pharmaceutical Association and Institute of Materia Medica, Chinese Academy of Medical Sciences.

https://doi.org/10.1016/j.apsb.2021.04.018

Supramolecule;
Molecular simulation

the inclusion mechanism played a primary role when STV in CD-MOF was at a low loading ratio, while the increasement in bioavailability at a high loading ratio, which was attributed to the nanocluster mechanism. This was confirmed by molecular simulation. In conclusion, CD-MOF is a promising system for STV loading, overcoming the insolubility and to improve the bioavailability of this natural compound.

1. Introduction

Isosteviol (STV) is a synthetic steviol glycoside derivative, which belongs to diterpene molecule[1]. STV exhibited a wide range of biological activities and pharmacological effects, including anti-fungal[2], anti-neoplastic[3−5], anti-viral[6,7], improving insulin sensitivity, reducing plasma triglycerides[8,9]. It also reduces vasoconstriction by the regulation of the ion channels and has cardioprotective effect against coronary reperfusion damage with little toxicity[10−12]. However, one drawback of STV's application as medicine could be its low solubility and low bioavailability[13]. At present, methods to improve the solubility of STV include: solid dispersion technology[14,15], the use of enzymes such as transglycosylase to improve solubility through regioselective enzymatic glycosylation[16−19], complexation with γ-cyclodextrin (γ-CD)[20], etc. There was no report on using the cyclodextrin metal-organic framework (CD-MOF) encapsulation of STV.

Using new materials and technologies to manufacture efficient, stable and safe drug carriers are popular strategies to develop new formulations in order to improve the stability, bioavailability and maximize efficacy. CD is a class of cyclic oligosaccharides conventionally used for decades to increase the solubility and bioavailability of insoluble drugs[21]. CDs are hollow cylindrical stereocyclic structures comprising of six, seven or eight D-glucopyranose units linked together, named as α-CD, β-CD and γ-CD, respectively, all with a hydrophobic inner lumen and hydrophilic outer surface[22−24]. Metal-organic framework (MOF), also named as porous coordination polymer (PCP), is three-dimensional reticular porous crystal materials composed of metal ions and organic ligands[25−28]. MOFs have received much attention due to their intrinsic tunable structure, high specific surface area, and various functionalities, and have become a rising star toward the domain of materials in the last two decades[27,29−31]. MOFs have been utilized in a wide range of fields, such as gas adsorption and separation[32−34], gas storage[35−37], memristors[38], catalysis[39−41], biosensors[42], chemical sensors[43], optical materials, molecular recognitions[44,45], biomedical imaging[46], food packaging[47], and drug delivery[48−50].

CD-MOF is infinitely extended and regularly arranged network-like porous crystalline materials with cyclodextrin as the organic ligand and alkali metal ions (K^+, Na^+, Rb^+) as the inorganic coupling units[51]. In recent years, the high drug loading capacity, the solubility enhancement capacity, the renewable, bio-degradable and the structural stability nature of CD-MOF have attracted widespread attention[52]. Notably, as a kind of porous material, CD-MOF has an advantage in terms of the number of pores and the tunability of pore size compared to activated carbon and zeolite materials. In addition, it has been reported that CD-MOF can control the drug release and mask the taste after forming host−guest complexes with drugs. For example, sodium diclofenac (DFNa) was loaded into different MOFs with γ-KCD, γ-NaCD and γ-FeCD by impregnation approach. The encapsulation rates (%) in KCD-MOF, NaCD-MOF and FeCD-MOF particles were 50 ± 0.015, 49 ± 0.109 and 55 ± 0.140, respectively[52]. This result manifested a good capacity of the γ-CD-MOF to incorporate the drugs with a high amount. Further, the *in vivo* anti-inflammatory activity showed that FeCD-MOF exhibits a pattern of controlled release of DFNa. The apparent solubility of azilsartan was greatly increased by CD-MOF loading, which was 340 times of the API, and the bioavailability was increased 9.7 times that of API in SD rats[53]. When CD-MOF was used for the encapsulation of two ester-based and two terpene-based fragrances, it was found that γ-CD-MOF nanocrystals had a higher encapsulation capacity for the two ester-based fragrances compared to γ-CD, with a good slow-release performance for all the fragrances tested[49]. In addition, vitamin A[54], curcumin[47], sucralose[55], and diflunisal were successfully loaded into CD-MOF. 5-Fluorouracil (5-FU) was loaded into β-CD-MOF by grinding method and reduced the cellular toxicity of the drug[56].

Hence, the selection of suitable CD-MOF material carriers is a very critical step and of great practical importance for poorly water-soluble drugs. In this paper, STV was investigated as the insoluble model drug and tried to be loaded into CD-MOF by solvent incubation method. Two different STV-CD loading molar ratios were achieved in CD-MOF (0.5:1 and 1:1). The oral bioavailability of STV@CD-MOF (1:1) was compared with that of STV@CD-MOF (0.5:1), STV@CD (0.5:1) and pure STV in SD rats. Different kinds of characterization techniques were performed to explore the mechanisms underlying in the enhancement of the solubility and bioavailability using CD-MOF.

2. Materials and methods

2.1. Materials

Isosteviol was obtained from Nanjing Spring & Autumn Biological Engineering Co., Ltd. (98%, Nanjing, China). γ-CD was purchased from Maxdragon Biochem Co., Ltd. (Guangdong,

China). The internal standard progesterone (Ourchem), potassium hydroxide (KOH), polyethylene glycol 20,000 (PEG20,000), methanol (MeOH), ethanol (EtOH) and other chemicals were provided by Sinopharm Chemical Reagent Co., Ltd. (Shanghai, China) and used in this study without further purification. Milli-Q water system (Millipore, Shanghai, China) was used in this study to obtain purified water.

2.2. Methods

2.2.1. Preparation of CD-MOF

The CD-MOF was synthesized from the previous procedure[57]. Concisely, 25.92 g γ-CD and 11.20 g KOH were weighed with the molar ratio $n_{\gamma\text{-CD}}$:n_{KOH} of 1:8, and were added into 800 mL of deionized water and then sonicated to dissolve as the mother liquor. Methanol of 480 mL was added into a glass reactor containing 800 mL of the mother liquor on a magnetic stirrer (RCT IKA, Staufen, Germany) at 400 rpm, 60 °C. It took approximately 20 min to make the system clear, thereafter 640 mg of PEG20,000 was added into the container. The reaction was continued for 10 min, until the solution became clear. The solution was then transferred into cold water at 15 °C for 2 h to obtain target crystals. The crystals were then centrifuged and washed twice each with anhydrous ethanol and methanol to remove the impurities. Ultimately, the CD-MOF was in the drying-oven (BPG-9140A, Shanghai Yiheng Technical Co., Ltd., Shanghai, China) at 80 °C for 2 h.

2.2.2. Preparation and optimization of STV@CD-MOF and STV@CD

STV@CD-MOF: STV-loaded CD-MOF (STV@CD-MOF) was developed using solvent incubation. Briefly, 1.82 g CD-MOF ($[K_2(C_{48}H_{80}O_{40})\ (OH)_2]_n$, MW = 1409.34)[58] was dispersed in 20 mL ethanol solution of STV at the concentration of 100 mg/mL (molar ratio of CD-MOF to STV was 1:5) and agitated at 60 °C with a speed of 400 rpm. To make the drug loading in MOF consistent with the γ-CD loading, the obtained product was washed with 5 mL ethanol, followed by filtering and vacuum drying (OZF-6050, Shanghai Yiheng Technical Co., Ltd., Shanghai, China) at 60 °C for 4 h to obtain STV@CD-MOF. When the washing condition to the product was considered as variable, other parameters involved such as temperature, mixing time, molar ratio and so forth were fixed as constants.

STV@CD: 1.30 g γ-CD was weighed, and dissolved in 100 mL water with sonication; 636.9 mg STV was added to 6.5 mL anhydrous ethanol and made sure to be dissolved completely, then added drop by drop to the above-mentioned γ-CD aqueous solution. It was agitated at 60 °C with a speed of 400 rpm for 4 h, followed by filtering, the supernatant was dried in a freeze dryer for 24 h at a drying temperature below −50 °C and a pressure below 20 Pa. It was evident that CD-MOF had great advantages in STV@CD-MOF preparation using the incubation method (8 h) over the freeze-drying method (28 h) for CD complexation.

To determine STV loading amount in STV@CD-MOF. 10 mg STV@CD-MOF sample was weighed and placed in a 25 mL volumetric flask, dissolved in methanol–water (50:50, *v*/*v*), following the obtained solution was centrifuged (12,000 rpm, 5 min; Micro 2R, Thermo Fisher Scientific) and the supernatant was taken for high-performance liquid chromatography (HPLC) analysis. The drug load was calculated as shown in Eq. (1)

$$\text{STV loading}\ (\%) = \frac{\text{STV measured in CD/CD} - \text{MOF}}{\text{weigh of STV@CD/CD} - \text{MOF}} \times 100 \quad (1)$$

Assay of STV was measured using HPLC (Agilent Technologies Inc. Santa Clara, CA, USA) on a Dikma Plastisil ODS C18 column (100 mm × 4.6 mm, 5 μm) with the column temperature of 40 °C. The mobile phases consisted of ACN-0.1% H_3PO_4 (70:30, *v*/*v*) with the flow rate of 0.8 mL/min. The injection volume was 20 μL and the detection wavelength was 210 nm. Chemstation software (Agilent) was utilized to reanalyze the chromatograms.

2.2.3. Solubility studies in vitro

The apparent solubility of STV, STV@KOH, STV@KOH-CD-MOF, and STV@CD in pH 1.0, pH 4.5, pH 6.8 and distilled water were determined. Excess STV (5 mg for STV raw material) and the above drug-loading samples (about 4, 8 and 20 mg drug content for STV@CD, STV@CD-MOF (0.5:1) and STV@CD-MOF (1:1), respectively) were placed in plastic centrifuge tubes, 1 mL water was added to prepare the supersaturated solution, which was placed in a constant temperature incubation shaker (ES-60þ, Wiggens, Germany) for 200 rpm at 25 °C for 2 h. The suspension was filtered through a 0.45 μm membrane to eliminate any insoluble particles.

The solubility of STV in different media was evaluated by HPLC−MS/MS using a Dikma Plastisil ODS C18 column (100 mm × 4.6 mm, 5 μm) at 40 °C. The chromatographic separation was performed by isocratic elution with the mobile phases of 0.1% formic acid aqueous solution and methanol (25:75) at the flow rate of 0.8 mL/min. The detection mode was multiple reaction monitoring method (MRM) in positive ion mode, and the transition of STV was *m*/*z* 319.2 → 273.2 with a collision energy (CE) of 16 eV. MassHunter V4.1 software (Agilent, USA) was used for data analysis in mass spectrometry mode. The solubility of each sample was measured in triplicates.

2.2.4. In vitro drug release

The dissolution of STV powder was determined by referring to the second method of dissolution and release determination in four parts of Chinese Pharmacopoeia (2020 edition). For the sake of investigating the release behaviors of STV in pH 1.0, pH 4.5, pH 6.8 and water, STV and related drug loaded samples were placed in 100 mL media at 50 rpm. Samples were extracted at points (5, 10, 20 and 30 min), then the entire release medium was replaced with 2 mL of the dissolution medium at the same temperature and inserted at the same time to maintain tank conditions. The extracted samples were filtered using 0.45 μm filter. Analysis was conducted as the conditions in Section 2.2.2. All experiments were made in triplicate.

2.2.5. Drug loading mechanism and molecular simulations

The field scanning emission electron microscope (SEM, S3400, Hitachi, Japan) and powder X-ray diffraction (PXRD, Bruker, USA) were conducted to characterize the morphology and crystallinity of the samples, respectively. The Synchrotron radiation-Fourier transform infrared spectroscopy (SR-FTIR) data were

obtained using a spectrometer (Nicolet 6700, Thermo Scientific, USA) at the Shanghai Synchrotron Radiation Facility (SSRF) with a range of 400−4000 cm^{-1}. The nitrogen adsorption−desorption isotherm and mean pore equivalent diameter were carried out using a porosimeter (Micromeritics, ASAP 2020, USA). Before the test, the samples were dried in vacuum at 60 °C for 4 h to remove residual solvent and water. Differential scanning calorimeter (DSC, PerkinElmer DSC8500, USA) was employed under nitrogen purge.

The molecular structure of STV was obtained from PubChem's open chemical database (PubChem CID: 99514). The original crystal structure of MOF was derived from the reported single crystal structure of CD-MOF-1. The automatic molecular docking calculation was carried out with the AutoDock Vina 1.1.2 docking program. Firstly, the STV model was prepared according to the energy minimization protocol. Then, the STV molecule was docked to γ-CD-MOF model. The docking result with maximum probability was used as the basis for subsequent structure optimization.

2.2.6. *In vivo characterization of STV@CD-MOF*

The male Sprague−Dawley (250 ± 50 g) was utilized and the rats were obtained from the Shanghai Jiesijie Laboratory Animals Co., Ltd. The study was approved by the Institutional Animal Care and Use Committee of Shanghai Institute of Materia Medica (IACUC Application No. 2020-04-ZJW-27, Shanghai, China).

The rats were divided into 4 groups randomly. Groups 1 to 4 were orally administered by STV, STV@CD, STV@CD-MOF (0.5:1) and STV@CD-MOF (1:1), respectively. The drug suspensions were prepared by dispersing in 0.5% sodium carboxymethyl cellulose (CMC-Na) and the dose was 4 mg/kg (calculated as STV). The rats were fasted for 12 h with free access to drinking water ahead of the experiments. Blood was collected into a centrifuge tube containing heparins from the orbits at indicated time point (0, 0.08, 0.16, 0.32, 0.75, 1, 2, 4, 6, 8, 10 and 24 h). Plasma was required by centrifugating (Thermo Fisher Scientific, 3500 rpm, 10 min), then cryo-preserved at −80 °C refrigerator.

Take the plasma sample out of the −80 °C refrigerator and set aside at ambient surroundings until melted. 80 μL of plasma sample was mixed with 10 μL of Progesterone (500 ng/mL) and 10 μL of solvent (methanol) were spun for 30 s, and finally 400 μL of acetonitrile (acetonitrile: acetic acid 95:5, *v*/*v*) was putted into and vortexed for 30 s. After blending, centrifugation (Thermo Fisher Scientific, 12,000 rpm, 5 min) was carried out for HPLC−MS/MS test.

2.2.7. *Determination of STV in plasma*

Blood concentrations were determined based on the results of HPLC−ESI-MS analysis on an Agilent HPLC system (Agilent, USA). The specific MS conditions were as described above. The transition of internal standard (progesterone) was *m*/*z* 315.2 → 97 with a collision energy (CE) of 20 eV. The STV had a good linearity in the range of 10.00−5000.00 ng/mL with the linear regression equation ($y = 1.064x-0.0885$) and correlation coefficient ($r = 0.995$). The lower limit of quantification (LLOQ) was 10 ng/mL with the RSD% lower than 20%. The precision values of low, middle and high concentrations were all lower than 15%, and the recoveries were within 95.30%−112.54%. These results met the requirements of the analytical method.

2.2.8. *Statistical methods*

The linearity of the calibration curves was verified using linear regression analysis, with STV expressed as mean ± standard deviation (SD), using *t*-test, all statistical analyses were performed using GraphPad prism 6.01 (GraphPad Software, Inc.). Pharmacokinetic parameters were computed and evaluated using DAS 2.0 software (Mathematical Pharmacology Professional Committee of China, Shanghai, China) for non-interval analysis. ***P value of 0.001 was deemed statistically significant.

3. Results and discussion

3.1. *Effective loading of STV*

The loadings of STV in CD-MOF were measured to be 11.6 ± 0.4% (STV@CD-MOF 0.5:1) and 19.0 ± 0.3% (STV@CD-MOF 1:1), wherein the distinction between them was washed or not (Fig. 1A). The drug loading of STV@CD-MOF decreased from 19.0% to 11.6% after washing. This also made the loading molar ratio of STV:CD-MOF from 1:1 to 0.5:1. And the drug loading of STV@CD (0.5:1) prepared using freeze drying method was equivalent with that of STV@CD-MOF (0.5:1) using solvent incubation method.

The cubical shaped CD-MOF is displayed in Fig. 1B. STV was incorporated into CD-MOF under agitation. SEM indicated that the morphology and size of CD-MOF remained unaltered when STV was incorporated. The morphology of STV@CD-MOF presented regular cubic with the size of 1−5 μm in the presence of different STV:CD molar ratios.

3.2. *Enhanced solubility of STV@CD-MOF*

STV compound was poor in solubility, and the current test methods failed to detect its solubility in acid (pH 1.0 and 4.5). The LLOQ was 20 ng/mL, and it can be assumed that the solubility of STV was less than 20 ng/mL except in pH 6.8 and water. As shown in Fig. 2, the solubilities of STV@CD-MOF in the four media were generally higher or similar to that of STV@CD. The solubility of STV@CD-MOF (2.60, 2.40, 10.98 and 19.96 mg/mL) at pH 1.0, 4.5, 6.8 and water were 3.4, 2.6, 3.9 and 24.9-fold higher than those of CD complexes (0.76, 0.93, 2.80 and 0.80 mg/mL), respectively. Compared with STV, its solubility was enhanced by as much as 154,000-fold in water, a similar increase of the solubility by 130,000-, 120,000- and 549,000-fold at pH 1.0, 4.5 and 6.8, respectively.

Compared with the solubility (239.9 μg/mL) of STV in KOH solution (pH 11), the structure of CD-MOF contributed primarily to drug solubility improvement. And the pH values of media were little changed by the addition of STV@CD-MOF samples after solubility test.

3.3. *pH-independent release behaviors of STV@CD-MOF*

From the dissolution analysis of STV@CD-MOF section, STV was minimally soluble in all four media and had a certain dependence on pH value. In contrast, the STV@CD-MOF (0.5:1) formulation significantly enhanced the release of STV, which was essentially complete release (100%) within 5 min in either water or in media with different pH, therefore it was non-pH dependent. The degree of drug release of STV@CD was 70%−80%, which

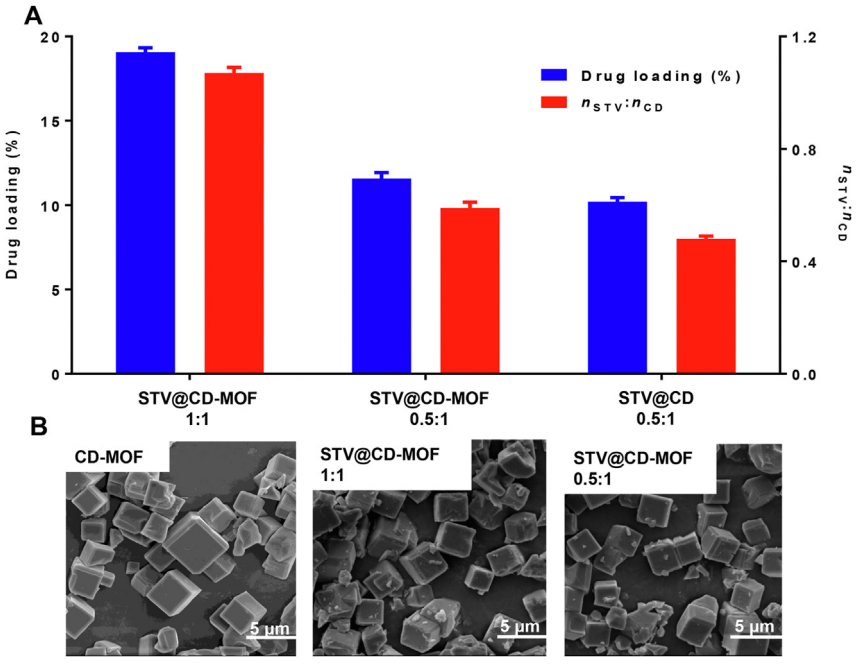

Figure 1 STV was efficiently incorporated into CD-MOF. (A) Efficient loading of STV by CD-MOF, (B) SEM images of CD-MOF, STV@CD-MOF (0.5:1), and STV@CD-MOF (1:1) (data are mean ± SD, $n = 3$). Scale bar = 5 μm.

was lower than that of STV@CD-MOF (0.5:1), underscoring the advantages of CD-MOF carriers. Notably, for the STV@CD-MOF 1:1, in which half (0.5:1) of STV was considered to be the inclusion of CD, and the other half (0.5:1) as nanoclusters of STV. The release profiles showed that a decreased release appeared at pH 1.0 and pH 4.5 (only about 40% of STV), while the cumulative release percentages in pH 6.8 and water were about 70%−80% (Fig. 3). This was attributed as nanoclusters formation in pH 1.0 and pH 4.5 to partially decrease the release, while the complexation form of STV in STV@CD-MOF (0.5:1) formulation showed instant and complete release in all media. The counter-intuitive release results between STV@CD-MOF (0.5:1) and STV@CD (0.5:1) were possibly caused by the structure and property of CD-MOF. CDs arrayed in CD-MOF regularly, which caused drug molecules more highly dispersed than that in CDs crystals during release.

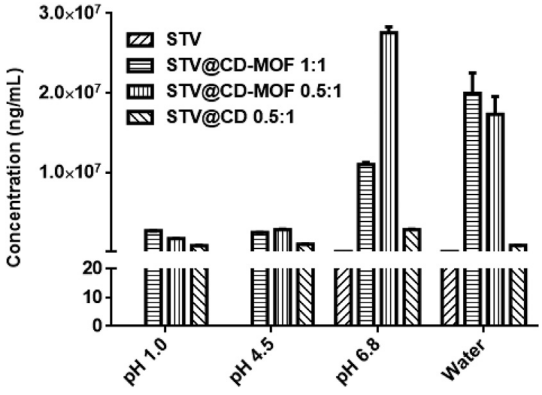

Figure 2 The solubility of STV@CD-MOF was significantly higher at different pH values compared to STV and STV@CD. The current HPLC method failed to detect STV solubility in pH 1.0 and pH 4.5, so the corresponding black column was not shown in Fig. 2 (data are mean ± SD, $n = 3$).

3.4. *Improved bioavailability of STV in rats*

The mean blood concentration time curves (Fig. 4) show the STV@CD, STV@CD-MOF (0.5:1) and STV@CD-MOF (1:1) groups achieved conspicuously rapid peak rates with high peak concentrations compared to the STV group.

The bioavailability of STV@CD and STV@CD-MOF (0.5:1) in rats was almost the same comparing the AUC after oral administration. Table 1 showed $AUC_{0-24\ h}$ of STV@CD-MOF (0.5:1) and STV@CD were 240.99 ± 55.39 and 232.00 ± 59.57 μg/mL·min, indicating the bioavailability of STV@CD group 4.61-fold greater compared to the free STV suspension (35.41 ± 27.77 μg/mL·min). The bioavailability of STV@CD-MOF (0.5:1) increased by 4.67-fold ($P < 0.001$) in comparison to free STV, however it was similar to STV@CD. This further demonstrated that the low drug loading molar ratio was the CD inclusion mechanism. The bioavailability of STV@CD-MOF (1:1) group ($AUC_{0-24\ h}$ = 307.25 ± 114.60 μg/mL·min) was 8.67-fold higher than that of STV ($P < 0.001$) and about 1.32-fold higher than STV@CD and STV@CD-MOF (0.5:1). It was not difficult to find the STV@CD-MOF (0.5:1) group had a shorter time to peak and higher peak concentrations compared to the STV@CD group and STV@CD-MOF (1:1), but the *in vivo* absorption and metabolite of STV in STV@CD-MOF (1:1) was prolonged in comparison with STV@CD and STV@CD-MOF (0.5:1). It was likely that the *in vivo* circumstance differed from the *in vitro* artificial media and the nano-clusters played a special role in absorption, which might be the reason that T_{max} of

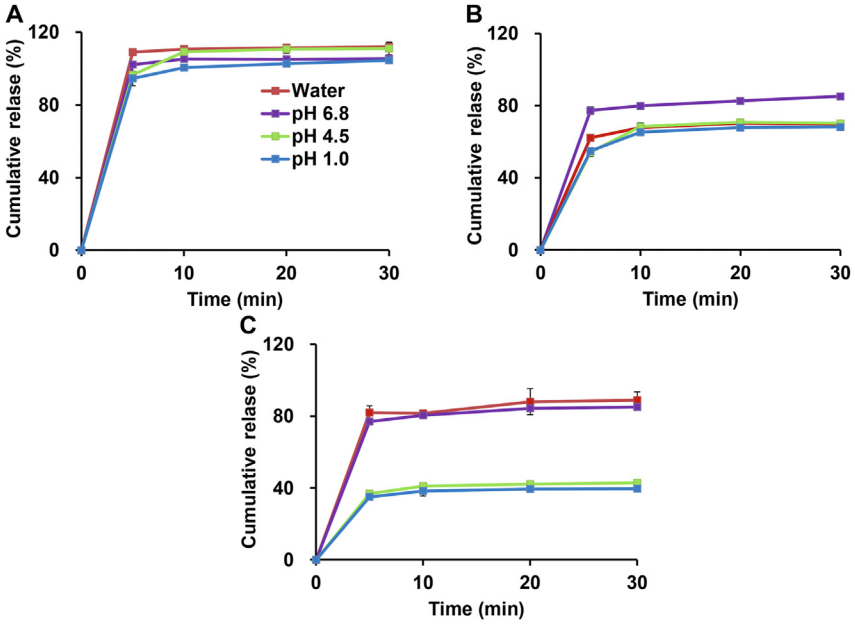

Figure 3 Drug release profiles of STV@CD-MOF (0.5:1) (A), STV@CD (B) and STV@CD-MOF (1:1) (C) in HCl solution at pH 1.0, acetate buffer at pH 4.5, phosphate buffer at pH 6.8 and water (data are mean ± SD, $n = 3$).

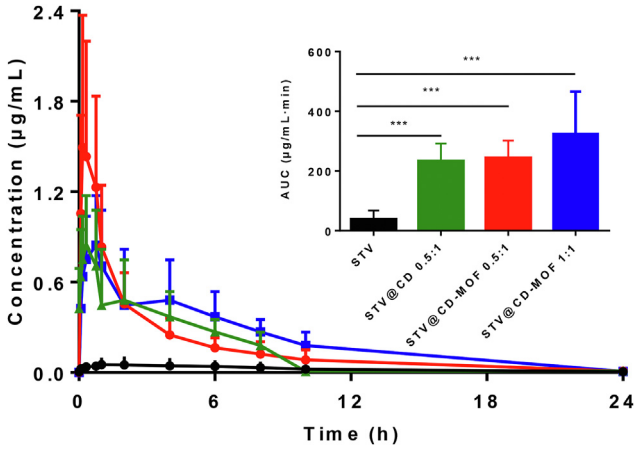

Figure 4 Plasma concentration−time profiles of STV in rats after oral administration of STV@CD-MOF (1:1), showing improved bioavailability in contrast to STV@CD-MOF (0.5:1), STV@CD and STV (data are mean ± SD, $n = 6$).

STV@CD-MOF (1:1) was almost 2-fold longer than STV@CD-MOF (0.5:1) and STV@CD. It was postulated that the nanoclusters formed in $(\gamma\text{-CD})_6$ facilitated its absorption and well exemplified on the basis of our preliminary works[53,59].

3.5. *Characterization and mechanism of STV@CD-MOF*

At present, the mechanism by which CD-MOF enhanced release *in vitro* and improved absorption *in vivo* has not been fully appreciated. It was argued that drug payload in CD-MOF was not only the role of CD encapsulation, but also the co-action of nanoclusters. Hence, in our study, STV@CD-MOF (1:1), STV@CD-MOF (0.5:1) and STV@CD were characterized in various aspects, including FTIR, PXRD, DSC, BET and molecular simulation to further manifest their encapsulation mechanism.

SR-FTIR: The characteristics of SR-FTIR spectrum (Fig. 5A) indicated that C═O stretching vibration peaks of the STV were 1735 cm^{-1} and 1693 cm^{-1} ($\nu_{C=O}$) characteristic absorption, the formation of STV@CD-MOF was verified by the C═O signals, where there was a shift from 1735 cm^{-1} to lower values (1727 or 1726 cm^{-1}) and/or there was no 1693 cm^{-1} peak. The C═O stretching vibration at 1735 cm^{-1} was shifted to 1727 cm^{-1} in STV@CD-MOF (0.5:1) and 1726 cm^{-1} in STV@CD (0.5:1), while there was almost no shift in STV@CD-MOF (1:1), but the absorption intensity diminished at 1735 cm^{-1} and was non-absorbing peak at 1693 cm^{-1}. The SR-FTIR spectra indicated that the interaction of STV in CD-MOF in STV@CD-MOF (0.5:1) was basically the same as that of the γ-CD complexation, probably due to the efficacious loading of STV, and the vibration of the characteristic peak of STV was masked. And the vibrations of

Table 1 Pharmacokinetic parameters of STV@CD-MOF, STV@CD and STV in rats.

Pharmacokinetic parameter	STV	STV@CD (0.5:1)	STV@CD-MOF (0.5:1)	STV@CD-MOF (1:1)
$AUC_{0-24\ h}$ (μg/mL·min)	35.41 ± 27.77	232.0 ± 59.6***	241.0 ± 55.4***	307.2 ± 114.6***
T_{max} (min)	180.3 ± 171.0	18.33 ± 9.83	11.67 ± 2.58	35.00 ± 12.25
C_{max} (μg/mL)	0.061 ± 0.039	0.918 ± 0.475	1.54 ± 0.85	0.84 ± 0.33

STV, isosteviol. Data are mean ± SD, $n = 6$. ***$P < 0.001$ *versus* STV.

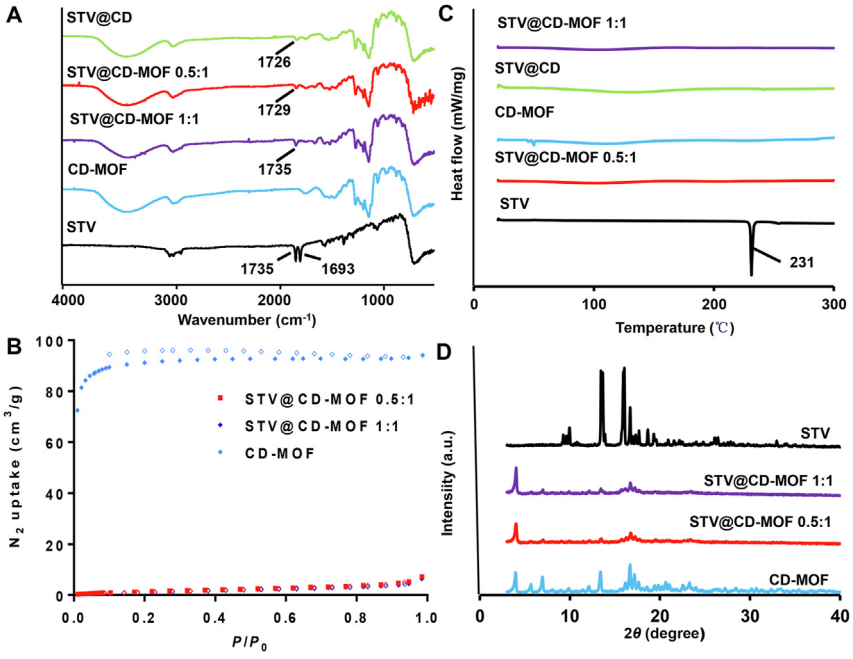

Figure 5 Characterizations and spectra of STV, CD-MOF, STV@CD, STV@CD-MOF (0.5:1), STV@CD-MOF (1:1). (A) FTIR, (B) DSC, (C) BET and (D) PXRD.

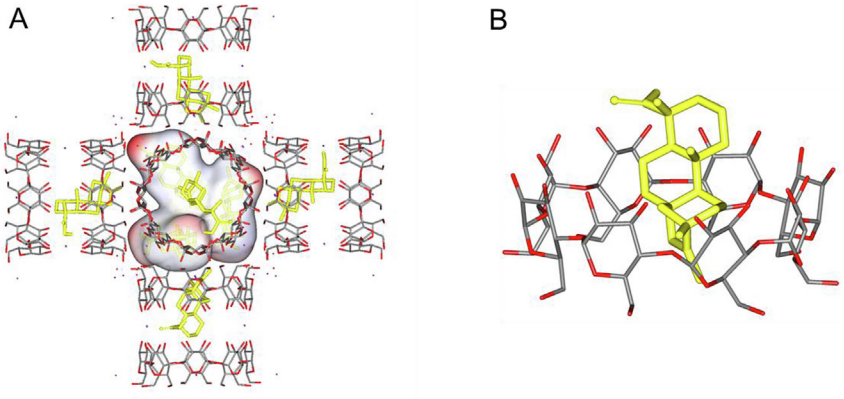

Figure 6 Molecular mechanism of STV distribution in CD-MOF as nano-cluster and CD complexation. (A) STV loaded in CD-MOF with a STV:CD molar ratio of 1:1 (polar hydrogen atoms were added on the carboxylic group). (B) The form of STV@CD-MOF presented after dissolving into water.

STV molecules in STV@CD-MOF (0.5:1) were more constrained by CD-MOF than those of STV molecules in STV@CD-MOF (1:1), resulting in a different chemical environment between the bicyclodextrin molecular pair and the cavity.

DSC: The thermal behavior of STV and STV-loadings were investigated by DSC (Fig. 5B). STV showed an intrinsic endothermic peak at 231 °C, which was determined by its melting point and crystalline character. Yet, it can be seen the characteristic peaks completely disappeared in STV@CD and STV@CD-MOF entirely in the range of 25−300 °C, which confirmed the successful packing of STV by CD-MOF and CD. Further, the absence of melting point in STV@CD-MOF indicated that the STV in CD-MOF and γ-CD converted crystal state to disordered amorphous state distributed in CD-MOF.

BET: The effect of STV on the porosity of CD-MOF was investigated by measuring the nitrogen adsorption capacity (Fig. 5C). The BET surface area of CD-MOF used in this study was estimated as 278.7 m^2/g. Drug molecules doping into CD-MOF were able to hinder the nitrogen uptake and led to the reduce of surface area, which could be used to confirm the interaction between CD-MOF and STV. As a result, the BET surface area of CD-MOF decreased to 6.6 m^2/g after drug loading, indicating that most of the pores of CD in CD-MOF were occupied by STV. At drug loading molar ratio of 1:1, the BET surface area of CD-MOF was

further decreased to 5.5 m^2/g. It was considered that more STV molecules entered into the cavities of CD-MOF.

PXRD: The PXRD patterns of STV@CD-MOF (0.5:1 and 1:1) all matched well with that of CD-MOF (Fig. 5D), indicating that the entry of STV into the nano-cavity of γ-CD-MOF would not destroy the crystal structure of CD-MOF. The characteristic peak of STV in STV@CD-MOF disappeared. The disappearance of STV PXRD peaks after drug loading indicated successful incorporation of STV in to the CD-MOF cavity.

Molecular docking mechanism of STV@CD-MOF: Drug molecules are more likely to stay in CD bimolecular pairs. Under these conditions, hydroxyl group of γ-CD formed hydrogen bonds with STV molecules, when the molar ratio of STV:CD was 0.5:1, and the bound free energy was −8.2 kcal/mol. If the drug molecules increased to molar ratio of STV:CD = 1:1, three STV molecules would take priority over existing in the large cavity of MOF in the form of nanocluster with extra molar ratio of about 0.5:1, and the hydrophilic groups of STV molecules interact with the hydrophilic hydroxyl groups on the inner surface of CD-MOF cavity with the free energy of binding varying from −6.7 to −8.4 kcal/mol (Fig. 6A). Of note, hydrogen bonds are the main interaction between STV and CD-MOF, while electrostatic interaction and coordination bonds between carboxylate groups and K^+ may also contribute to the adsorption energy. In STV@CD-MOF, CD-MOF was soluble in water, and there were STV@CD and STV nanoclusters in the solution system. The apparent solubility of STV was significantly increased when STV@CD and nanoclusters released once STV@CD-MOF dissolved into water, which also increased rate of encapsulation of CD by virtue of increasing contact area. In the STV@CD complex, STV was encapsulated by CD with the molar ratio STV:CD being 1:1 (Fig. 6B). In conclusion, it was considered that ionization and cyclodextrin inclusion synergistically enhanced the solubility of the drug in water, while the CD-MOF complex markedly augmented the rate of the CD inclusion process described above.

4. Conclusions

Many natural compounds such as STV are limited in application due to low bioavailability and poor solubility. To enhance solubility and bioavailability is crucial to the formulation development regarding STV. In this context, loading of STV molecules into nano-architectures in the superhydrophilic CD-MOF had the advantages over conventional γ-CD complexation. CD-MOF not only had the high drug loading efficiency but also the simplicity of the preparation process. Using CD-MOF as a supramolecular carrier, the solubilities of STV in varied media were significantly improved and the releasing profiles significantly improved in a non-pH-dependent way. Worthy of note, STV@CD-MOF (1:1) revealed the betterment of bioavailability in comparison to STV@CD. The STV loading position and nanocluster formation in CD-MOF had beneficial contribution to the solubility and bioavailability, which may be superior to CD inclusion. This superiority was explored using molecular simulations and confirmed by pharmacokinetics *in vivo*. In conclusion, this study demonstrated that CD-MOF is a useful formulation strategy to upgrade a drug candidate, which is insoluble either in acid media or in water.

Acknowledgements

The authors are grateful for the financial support from the National Science Foundation for Young Scientists of China (No. 81803441), the National Science and Technology Major Projects for the Major New Drugs Innovation and Development (No. 2018ZX09721002-009, China), the National Natural Science Foundation of China (No. 81873019) and the University Synergy Innovation Program of Anhui Province (GXXT-2020-025). Thanks go to the staffs from BL01B beamline of National Facility for Protein Science Shanghai (NFPS) at Shanghai Synchrotron Radiation Facility for their assistance in SR-FTIR measurement.

Author contributions

Jiwen Zhang, Li Wu and Shuangying Gui designed the research. Xiaojin Chen, Tao Guo, Kaikai Zhang and Jiacai Chen carried out the experiments and performed data analysis. Caifen Wang, Xiaohong Ren, Qin Wang, Yingchao Yang and Chongjing Liu participated part of the experiments. Xiaojin Chen, Tao Guo and Kaikai Zhang wrote the manuscript. Wen Tan, Shuangying Gui, Li Wu and Jiwen Zhang revised the manuscript. All of the authors have read and approved the final manuscript.

Conflicts of interest

The authors have no conflicts of interest to declare.

References

1. Gu WQ, Rebsdorf A, Hermansen K, Gregersen S, Jeppesen PB. The dynamic effects of isosteviol on insulin secretion and its inability to counteract the impaired beta-cell function during gluco-, lipo-, and aminoacidotoxicity: studies *in vitro*. *Nutrients* 2018;**10**:13.
2. Abdullah Al-Dhabi N, Valan Arasu M, Rejiniemon TS. *In vitro* antibacterial, antifungal, antibiofilm, antioxidant, and anticancer properties of isosteviol isolated from endangered medicinal plant pittosporum tetraspermum. *Evid Based Complement Alternat Med* 2015;**2015**:164261.
3. Malki A, El-Sharkawy A, El Syaed M, Bergmeier S. Antitumor activities of the novel isosteviol derivative 10C against liver cancer. JAr *Anticancer Res* 2017;**37**:1591−601.
4. Liu CJ, Zhang T, Yu SL, Dai XJ, Wu Y, Tao JC. Synthesis, cytotoxic activity, and 2D- and 3D-QSAR studies of 19-carboxyl-modified novel isosteviol derivatives as potential anticancer agents. *Chem Biol Drug Des* 2017;**89**:870−87.
5. Liu C, Yu S, Liu Y, Dai X, Wu Y, Li R, et al. Synthesis, cytotoxic activity evaluation and HQSAR study of novel isosteviol derivatives as potential anticancer agents. *Eur J Med Chem* 2016;**115**:26−40.
6. Huang T, Chou B, Lin C, Weng J, Chou C, Yang L, et al. Synthesis and antiviral effects of isosteviol-derived analogues against the hepatitis B virus. *Phytochemistry* 2014;**99**:107−14.
7. Huang TJ, Yang CL, Kuo YC, Chang YC, Yang LM, Chou BH, et al. Synthesis and anti-hepatitis B virus activity of C4 amide-substituted isosteviol derivatives. *Bioorg Med Chem* 2015;**23**:720−8.
8. Ruiz-Ruiz J, Moguel-Ordoñez Y, Segura-Campos M. Biological activity of stevia rebaudiana bertoni and their relationship to health. *Crit Rev Food Sci* 2017;**57**:2680−90.

9. Carrera-Lanestosa A, Moguel-Ordóñez Y, Segura-Campos M. Stevia rebaudiana Bertoni: a natural alternative for treating diseases associated with metabolic syndrome. *J Med Food* 2017;**20**:933−43.
10. Mathur S, Bulchandani N, Parihar S, Shekhawat GS. Critical review on steviol glycosides: pharmacological, toxicological and therapeutic aspects of high potency zero caloric sweetener. *Int J Pharm* 2017;**13**:916−28.
11. Adehin A, Tan KS, Tan W. Erythrocyte partitioning profile of isosteviol in human and rat blood. *Curr Ther Res Clin E* 2019;**91**:1−4.
12. Adehin A, Tan KS, Lu ZQ, Cheng Q, Tan W. *In vitro* metabolic stability and biotransformation of isosteviol in human and rat liver fractions. *Drug Metabol Pharmacokinet* 2019;**34**:194−200.
13. Yin C, Chen Y, Wu H, Xu D, Tan W. Attenuation of ischemia/reperfusion-induced inhibition of the rapid component of delayed rectifier potassium current by Isosteviol through scavenging reactive oxygen species. *Bba-Biomembranes* 2017;**1859**:2447−53.
14. Hui H, Ou SX, Fang T, Hao Z, Qing L, Wen T. Neuroprotective effects of isosteviol sodium injection on acute focal cerebral ischemia in rats. *Oxid Med Cell Longev* 2016;**2016**:1379162.
15. Pang S, Ma C, Zhang N. Investigation of the solubility enhancement mechanism of rebaudioside D using a solid dispersion technique with potassium sorbate as a carrier. *Food Chem* 2015;**174**:564−70.
16. Lu T, Xia Y. Transglycosylation specificity of glycosyl donors in transglycosylation of stevioside catalysed by cyclodextrin glucanotransferase. *Food Chem* 2014;**159**:151−6.
17. Wan HD, Xia YM. Enzymatic transformation of stevioside using a beta-galactosidase from sulfolobus sp. *Food Funct* 2015;**6**:3291−5.
18. Musa A, Miao M, Zhang T, Jiang B. Biotransformation of stevioside by Leuconostoc citreum SK24.002 alternansucrase acceptor reaction. *Food Chem* 2014;**146**:23−9.
19. Lemus-Mondaca R, Vega-Galvez A, Zura-Bravo L, Ah-Hen K. Stevia rebaudiana bertoni, source of a high-potency natural sweetener: acomprehensive review on the biochemical, nutritional and functional aspects. *Food Chem* 2012;**132**:1121−32.
20. Wan HD, He GZ, Zhang HJ. Isosteviol preparation and inclusion complexation of it with cyclodextrin. *J Incl Phenom Macro* 2019;**94**:65−73.
21. Zhou JW, Ritter H. Cyclodextrin functionalized polymers as drug delivery systems. *Polym Chem* 2010;**1**:1552−9.
22. Davis ME, Brewster ME. Cyclodextrin-based pharmaceutics: past, present and future. *Nat Rev Drug Discov* 2004;**3**:1023−35.
23. Shelley H, Babu RJ. Role of Cyclodextrins in nanoparticle-based drug delivery systems. *J Pharmacol Sci* 2018;**107**:1741−53.
24. Crini G. Review: a history of cyclodextrins. *Chem Rev* 2014;**114**:10940−75.
25. Li H, Eddaoudi M, O'Keeffe M, Yaghi OM. Design and synthesis of an exceptionally stable and highly porous metal-organic framework. *Nature* 1999;**402**:276−9.
26. Ferey G. Hybrid porous solids: past, present, future. *Chem Soc Rev* 2008;**37**:191−214.
27. Deng HX, Doonan CJ, Furukawa H, Ferreira RB, Towne J, Knobler CB, et al. Multiple functional groups of varying ratios in metal-organic frameworks. *Science* 2010;**327**:846−50.
28. O'Keeffe M, Peskov MA, Ramsden SJ, Yaghi OM. The reticular chemistry structure resource (RCSR) database of, and symbols for, crystal nets. *Acc Chem Res* 2008;**41**:1782−9.
29. Liu YL, Eubank JF, Cairns AJ, Eckert J, Kravtsov VC, Luebke R, et al. Assembly of metal-organic frameworks (MOFs) based on indium-trimer building blocks: a porous MOF with soc topology and high hydrogen storage. *Angew Chem Int Ed* 2007;**46**:3278−83.
30. O'Keeffe M, Yaghi OM. Deconstructing the crystal structures of metal-organic frameworks and related materials into their underlying nets. *Chem Rev* 2012;**112**:675−702.
31. Zheng HQ, Liu CY, Zeng XY, Chen J, Lu J, Lin RG, et al. MOF-808: a metal-organic framework with intrinsic peroxidase-like catalytic activity at neutral pH for colorimetric biosensing. *Inorg Chem* 2018;**57**:9096−104.
32. Gould JA, Athwal HS, Blake AJ, Lewis W, Hubberstey P, Champness NR, et al. Gas adsorption and structural diversity in a family of Cu(II) pyridyl-isophthalate metal-organic framework materials. *Philos T R Soc B* 2017;**375**:16.
33. Li L, Lin R, Krishna R, Li H, Xiang S, Wu H, et al. Ethane/ethylene separation in a metal-organic framework with iron-peroxo sites. *Science* 2018;**362**:443−6.
34. Wang L, Liang XY, Chang ZY, Ding LS, Zhang S, Li BJ. Effective formaldehyde capture by green cyclodextrin-based metal-organic framework. *ACS Appl Mater Interfaces* 2018;**10**:42−6.
35. Furukawa H, Cordova KE, O'Keeffe M, Yaghi OM. The chemistry and applications of metal-organic frameworks. *Science* 2013;**341**:974.
36. Murray LJ, Dincă M, Long JR. Hydrogen storage in metal-organic frameworks. *Chem Soc Rev* 2009;**38**:1294−314.
37. Latroche M, Surble S, Serre C, Mellot-Draznieks C, Llewellyn PL, Lee JH, et al. Hydrogen storage in the giant-pore metal-organic frameworks MIL-100 and MIL-101. *Angew Chem Int Ed* 2006;**45**:8227−31.
38. Yoon SM, Warren SC, Grzybowski BA. Storage of electrical information in metal-organic-framework memristors. *Angew Chem Int Ed* 2014;**53**:4437−41.
39. Sabo M, Henschel A, Froede H, Klemm E, Kaskel S. Solution infiltration of palladium into MOF-5: synthesis, physisorption and catalytic properties. *J Mater Chem* 2007;**17**:3827−32.
40. Mon M, Rivero-Crespo MA, Ferrando-Soria J, Vidal-Moya A, Boronat M, Leyva-Pérez A, et al. Synthesis of densely packaged, ultrasmall PtO_2 Clusters within a thioether-functionalized mof: catalytic activity in industrial reactions at low temperature. *Angew Chem* 2018;**130**:6294−9.
41. Li J, Ren Y, Qi C, Jiang H. A chiral salen-based MOF catalytic material with high thermal, aqueous and chemical stabilities. *Dalton Trans* 2017;**46**:7821−32.
42. Fang X, Zong B, Mao S. Metal-organic framework-based sensors for environmental contaminant sensing. *Nano-Micro Lett* 2018;**10**:64.
43. Kreno LE, Leong K, Farha OK, Allendorf M, Van Duyne RP, Hupp JT. Metal-organic framework materials as chemical sensors. *Chem Rev* 2012;**112**:1105−25.
44. Shekhah O, Wang H, Paradinas M, Ocal C, Schupbach B, Terfort A, et al. Controlling interpenetration in metal-organic frameworks by liquid-phase epitaxy. *Nat Mater* 2009;**8**:481−4.
45. Deng HX, Grunder S, Cordova KE, Valente C, Furukawa H, Hmadeh M, et al. Large-pore apertures in a series of metal-organic frameworks. *Science* 2012;**336**:1018−23.
46. Zhuang J, Young AP, Tsung CK. Integration of biomolecules with metal-organic frameworks. *Small* 2017;**13**:14.
47. Moussa Z, Hmadeh M, Abiad MG, Dib OH, Patra D. Encapsulation of curcumin in cyclodextrin-metal organic frameworks: dissociation of loaded CD-MOFs enhances stability of curcumin. *Food Chem* 2016;**212**:485−94.
48. Wang L, Zheng M, Xie Z. Nanoscale metal-organic frameworks for drug delivery: a conventional platform with new promise. *J Mater Chem B* 2018;**6**:707−17.
49. Zhang B, Huang J, Liu K, Zhou Z, Jiang L, Shen Y, et al. Biocompatible cyclodextrin-based metal-organic frameworks for long-term sustained release of fragrances. *Ind Eng Chem Res* 2019;**58**:19767−77.
50. Agostoni V, Chalati T, Horcajada P, Willaime H, Gref R. Towards an improved anti-hiv activity of nrti *via* metal-organic frameworks nanoparticles. *Adv Healthc Mater* 2013;**2**:1630−7.
51. Forgan RS, Smaldone RA, Gassensmith JJ, Furukawa H, Cordes DB, Li Q, et al. Nanoporous carbohydrate metal-organic frameworks. *J Am Chem Soc* 2011;**134**:406−17.
52. Abucafy MP, Caetano BL, Chiari-Andreo BG, Fonseca-Santos B, do Santos AM, Chorilli M, et al. Supramolecular cyclodextrin-based metal-organic frameworks as efficient carrier for anti-inflammatory drugs. *Eur J Pharm Biopharm* 2018;**127**:112−9.
53. He Y, Zhang W, Guo T, Zhang G, Qin W, Zhang L, et al. Drug nanoclusters formed in confined nano-cages of CD-MOF: dramatic enhancement of solubility and bioavailability of azilsartan. *Acta Pharm Sin B* 2019;**9**:97−106.

54. Zhang G, Meng F, Guo Z, Guo T, Peng H, Xiao J, et al. Enhanced stability of vitamin A palmitate microencapsulated by gamma-cyclodextrin metal-organic frameworks. *J Microencapsul* 2018;**35**:249−58.
55. Lv N, Guo T, Liu B, Wang C, Singh V, Xu X, et al. Improvement in thermal stability of sucralose by gamma-cyclodextrin metal-organic frameworks. *Pharm Res* 2017;**34**:269−78.
56. Sha J, Wu L, Li S, Yang X, Zhang Y, Zhang Q, et al. Synthesis and structure of new carbohydrate metal-organic frameworks and inclusion complexes. *J Mol Struct* 2015;**1101**:14−20.
57. Liu B, Li H, Xu X, Li X, Lv N, Singh V, et al. Optimized synthesis and crystalline stability of γ-cyclodextrin metal-organic frameworks for drug adsorption. *Int J Pharm* 2016;**514**:212−9.
58. Smaldone RA, Forgan RS, Furukawa H, Gassensmith JJ, Slawin AMZ, Yaghi OM, et al. Metal-organic frameworks from edible natural products. *Angew Chem Int Ed* 2010;**49**:8630−4.
59. Xu J, Wu L, Guo T, Zhang G, Wang C, Li H, et al. A "Ship-in-a-Bottle" strategy to create folic acid nanoclusters inside the nanocages of gamma-cyclodextrin metal-organic frameworks. *Int J Pharm* 2019;**556**:89−96.